Available online at www.sciencedirect.com
SCIENCE DIRECT®
Journal of the Mechanics and Physics of solids
53 (2005) 1314–1333
JOURNAL OF THE MECHANICS AND PHYSICS OF SOLIDS
www.elsevier.com/locate/jmps

Experiments and modeling of carbon nanotube-based NEMS devices

C.-H. Ke[1], N. Pugno[1,2], B. Peng, H.D. Espinosa*

Department of Mechanical Engineering, Northwestern University, Evanston, IL 60208-3111, USA

Received 24 August 2004; received in revised form 20 January 2005; accepted 24 January 2005

Abstract

In this paper, carbon nanotube-based nanoelectromechanical systems (NEMS) are nanofabricated and tested. In-situ scanning electron microscopy measurements of the deflection of the cantilever under electrostatic actuation are reported. In particular, a cantilever nanotube suspended over an electrode (nanoswitch), or two symmetric cantilever nanotubes (nanotweezers), from which a differential in electrical potential is imposed, are studied. The finite deformation regime investigated here is the first of its kind. An analytical model based on the energy method in both small deformation and finite kinematics (large deformation) regimes is used to interpret the measurements. The theory overcomes limitations of prior analysis reported in the literature towards the prediction of the structural behavior of NEMS. Some of the simplifying hypotheses have been removed. Furthermore, the theory takes into account the cylindrical shape of the deflected nanotube in the evaluation of its electrical capacitance, the influence of the van der Waals forces as well as finite kinematics. In addition, tip charge concentration and a quantum correction of the electrical capacitance are also considered. The energy-based method is used to predict the structural behavior and instability of the nanotube, corresponding to the on/off states of the nanoswitch, or to the open/close states of the nanotweezers—at the so-called pull-in voltage. Accuracy of the derived formulas is assessed by comparison of the theoretical prediction and experimental data in both small deformation and finite kinematics regimes. The results reported in this work are

*Corresponding author. Tel.: +1 8474675989; fax: +1 8474913915.
E-mail address: espinosa@northwestern.edu (H.D. Espinosa).
[1]These two authors contributed equally to this work.
[2]On leave from Department of Structural Engineering, Politecnico di Torino, Torino, Italy.

doi:10.1016/j.jmps.2005.01.007

particularly useful in the characterization of the electromechanical properties of nanotubes as well as in the optimal design of nanotube-based NEMS devices.

Keywords: Carbon nanotubes; NEMS; Nanoswitch; Nanotweezers; Energy method; Finite kinematics

1. Introduction

Ever since their discovery (Iijima, 1991), carbon nanotubes (CNTs) have been attracting major interest in the scientific community. In the last decade, the mechanical and electronic properties of nanotubes have been investigated. Small size, low density, high stiffness, flexibility and strength, as well as excellent electronic properties and unique coupled electromechanical behaviors (Tombler et al., 2000; Johnson et al., 2004; Liu et al., 2004), suggest that nanotubes have the potential to impact the development of novel composites, electronic devices and nanoelectromechanical systems (NEMS). Nanotubes (as well as nanoropes—composed of several nanotubes—and nanowires—having different shaped compact cross-sections) are envisioned as the ultimate fiber reinforcements as a consequence of their extremely high stiffness (Young's modulus of the order of 1 TPa, Treacy et al., 1996; Chopra and Zettl, 1998) and flexibility (strain at tensile failure of the order of 30%, Yakobson et al., 1997). Their strength, recently investigated in the work by Yu et al. (2000), is of the order of 10–100 GPa. For a recent review on the mechanics of carbon nanotubes the reader should refer to the paper by Qian et al. (2002).

Recently some research groups have been able to manufacture NEMS devices. For instance, Kim and Lieber (1999) developed nanotweezers. The mechanical capabilities of the nanotweezers were demonstrated by gripping and manipulating submicron clusters and nanowires. Likewise, Rueckes et al. (2000) investigated a carbon nanotube-based nonvolatile random access memory, by considering an innovative bistable nanoswitch based on electrostatic and van der Waals forces. The authors emphasized the extreme high integration level of the nanoswitches approaching 10^{12} elements per cm^2 and an element operation frequency in excess of 100 GHz. The viability of the concept was demonstrated by the experimental realization of a reversible bistable nanotube-based bit. Furthermore, the first really true nanotube-based NEMS, fully integrating electronic control and mechanical response, was developed only recently (Fennimore et al., 2003) by realization of a rotational motor. The authors reported the construction and successful operation of a fully synthetic nanoscale electromechanical motor incorporating a rotational metal plate, with a multi-walled carbon nanotube serving as the key motion-enabling element.

In spite of this fast acceleration in the development of NEMS structures, the amount of experimental data is extremely limited due to the complexity involved in the realization of nanodevices. Likewise, accurate analyses and formulas needed in the design of NEMS are still lacking. The first extensive investigation of the behavior of NEMS devices has been recently reported by Desquenes et al. (2002). In that paper, the equation of the elastic line of a nanotube suspended over an electrode and from which a

differential electrical potential is imposed, was numerically solved according to continuum mechanics, assuming small displacements. The corresponding pull-in voltages, at the structural instability, were evaluated for different cases. In addition, the first attempt to obtain an analytical formula for the pull-in voltage of the nanotube was also proposed, assuming for the nanotube a plate-like undeformed shape connected via a lumped stiffness to the ground electrode. As emphasized by the same authors, the proposed formula was not able to accurately reproduce all their numerical results.

In this paper we investigate the electromechanical behavior of CNT-based NEMS by means of experimentation, in a regime until now unexplored, and by performing a theoretical analysis in both small deformation and finite kinematics (large deformation) regimes. In-situ scanning electron microscopy (SEM) experiments of electrostatically actuated nanotube cantilevers, in the finite kinematics regime, are described. Experimental data concerning the continuous deflection is reported and contrasted with the small deformation regime data reported by Akita et al. (2001) (nanotweezers). The experiments are analyzed by means of an energy-based theory. Through this theory, the continuous deflection and pull-in voltage of the nanotube device are predicted. The model takes into account the cylindrical shape of the deflected nanotube in the evaluation of its electrical capacitance, the influence of van der Waals forces, finite kinematics, quantum correction to the electrical capacitance and tube tip charge concentration. A comparison between experimental data and theoretical predictions, in both small deformation and finite kinematics regimes, is discussed. The errors from neglecting charge concentration and finite deformation effects are also discussed.

2. Experiments

2.1. Small deformation regime

One of the few experimental results on in-situ SEM electrostatic actuation of carbon nanotube devices was reported by Akita et al. (2001). They employed two single-clamped nanotube cantilevers placed parallel to each other to construct nanotweezers. The length of the nanotube cantilever employed in the experiments was 2.5 μm and the gap between them was 780 nm. Theoretically, this is equivalent to a single-clamped nanotube with a length of 2.5 μm freestanding above an infinite large conductive substrate at a distance of 390 nm. Because the ratio between the length of the nanotube and the gap between nanotube and electrode is 6.4, finite kinematics effects are expected to be negligible; hence, the measured deflection of the nanotube under the electrostatic force can be considered in the small deformation regime. The gap-voltage measurements reported by Akita et al. (2001) are later plotted and compared to the theoretical analysis results (see Section 4).

2.2. Finite kinematics regime

In this section, we describe in-situ SEM experiments performed on CNT cantilevers using the setup schematically shown in Fig. 1. Multi-walled carbon nanotubes

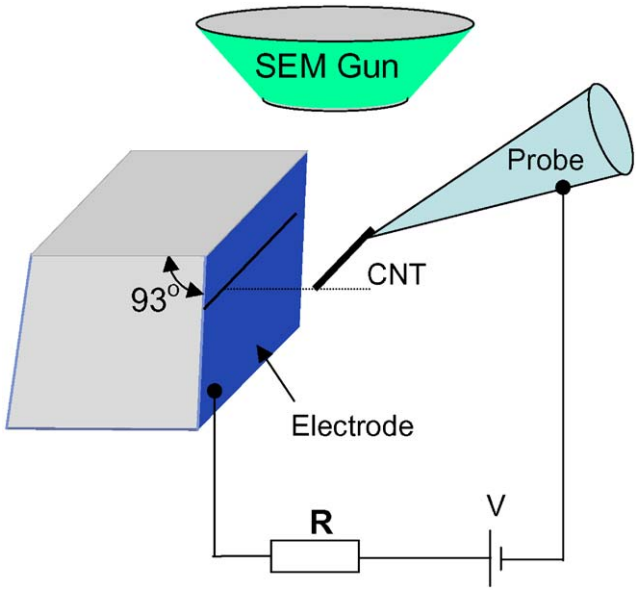

Fig. 1. Schematic of the experimental configuration employed in the electrostatic actuation of MWCNTs.

(MWCNTs) from Alfa Aesar were used. Since these nanotubes are provided in bundles, they were first separated by a few hours of ultrasonication in an aqueous dispersant commercially available from Alfa Aesar. A droplet of solution was then placed on a copper transmission electron microscope (TEM) grid and dried. By employing a 3-axes nanomanipulator from Klocke Co., possessing sub-nanometer resolution, CNTs were manipulated and mounted on the tip of the manipulator probe inside a dual-beam scanning electron microscopy (SEM)/focused ion beam (FIB) chamber (FEI Dual-Beam 235 FIB). The TEM grid was examined using SEM and protruding nanotubes were identified. By approaching the nanomanipulator tungsten (W) tip to a protruding and straight nanotube, good contact between the tip and nanotube was made. Such contact was assessed from the motion of the nanotube while slightly lifting the probe. Electron beam-induced deposition (EBID) of platinum (Pt) was then employed to weld the nanotube to the probe. The probe was then displaced to pull out the nanotube from the grid and in doing so a cantilever sample was obtained. Fig. 2 shows a CNT cantilever with the fixed end welded to the tip of the nanomanipulator probe. The length of the nanotube was measured at high magnification to be about 6.8 μm.

The electrode employed in the configuration shown in Fig. 1 was a piece of silicon wafer coated with 50 nm Au film by electron beam evaporation. This Si chip was attached onto the side of a Teflon block possessing an angle of 93° between the top and bottom surfaces. The nanotube cantilever shown in Fig. 2 was then placed horizontal and parallel to the electrode surface as schematically shown in Fig. 1. The distance between the top surface and the gun was 5 mm, while the distance between the nanotube and the gun was measured to be 6.8 mm. By focusing on the electrode

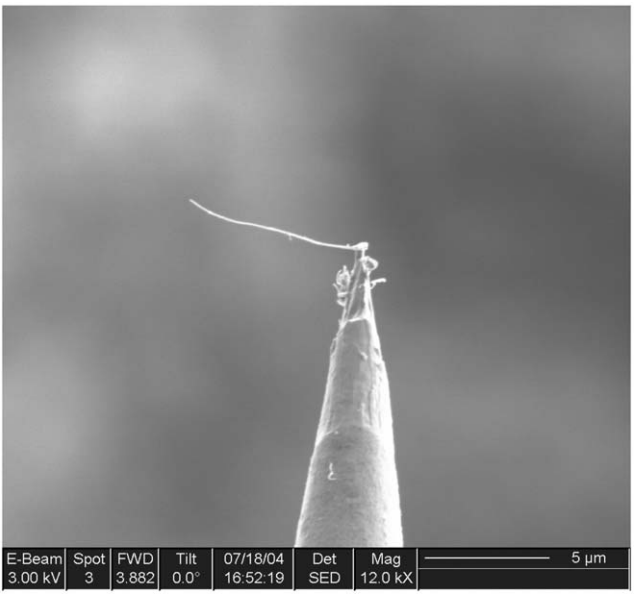

Fig. 2. SEM image of a carbon nanotube mounted at the tip of the nanomanipulator probe.

surface and adjusting the working distance to be 6.8 mm, a feature on the electrode, which is on the same horizontal plane with the nanotube, was located. Such a feature is schematically marked as a line in Fig. 1. The horizontal distance between the nanotube and the line was controlled by the nanomanipulator and set to 3 μm . In the circuit, a resistor $R = 1.7\,\mathrm{M\Omega}$ was employed to limit the current. Because the ratio between the length of the nanotube and the gap between the nanotube and electrode is 2.3, the deflection of the nanotube under electrostatic force can be considered to be in the finite kinematics regime.

Figs. 3(A–E) show the scanning electron images of the deflection of the CNT as it is subjected to increasing applied voltages. The feature on the electrode, which is in the same horizontal plane containing the cantilever nanotube, is schematically marked as a solid black line in Figs. 3(A–E). These images clearly reveal changes in nanotube deflection and local curvature as a function of applied voltage. A very noticeable effect, although difficult to quantify accurately, is the changes in local curvature. The pull-in voltage, V_{PI}, was measured to be 48 V. Through digital image processing, the tip deflection as a function of voltage was measured. The gap-voltage measurements are later plotted and compared to the theoretical analysis results (see Section 4).

3. Modeling: electrostatic and van der Waals energies

We focus our attention on a cantilever nanotube suspended over a graphitic electrode at a distance $r = H$ from which a difference V in the electrostatic potential

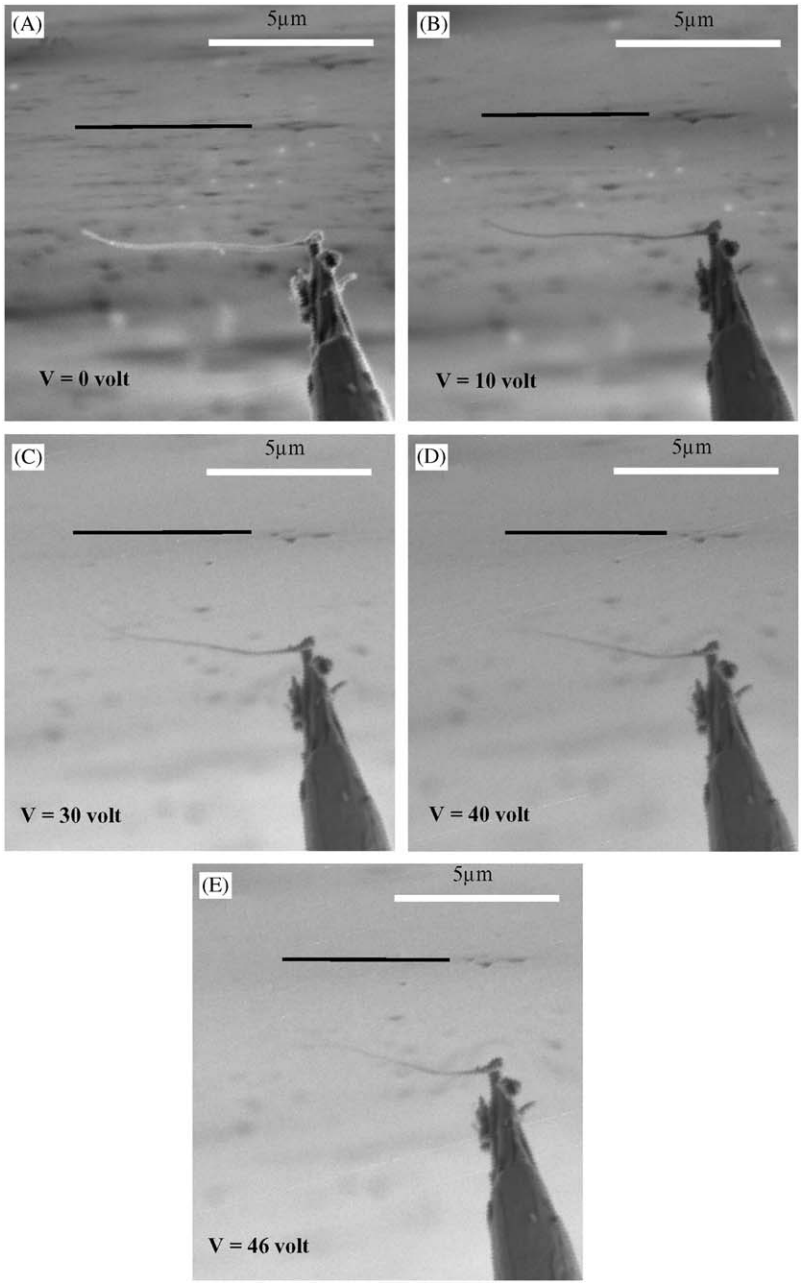

Fig. 3. SEM images of the deformed carbon nanotube at various biased voltages.

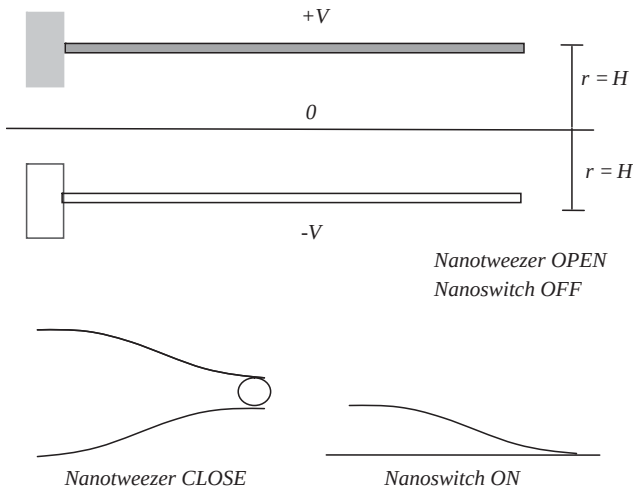

Fig. 4. Schematics of nanoswitch and nanotweezers.

is imposed (e.g. in a nanoswitch or nanotweezers). Note that this is equivalent to the problem of two identical cantilever nanotubes placed at distance $2r = 2H$ under a difference in voltage of $2\,V$, as imposed by the symmetry. The two schemes are shown in Fig. 4 and correspond to the experimental setups discussed in Section 2.

3.1. General expressions

The electrostatic forces between two oppositely charged structures can be computed by using a standard capacitance model assuming perfect conductors. This implies that the electrostatic potential is constant in the two structures. Consequently, the electrostatic energy can be evaluated as

$$E_{\text{elec}} = \tfrac{1}{2}CV^2, \tag{1}$$

where V is the difference in voltage and C is the capacitance, defined as $C = Q/V$, $\mp Q$ being the two opposite total charges in the two conductors. For a double-layer conductor, the contribution to the capacitance of two infinitesimal surfaces oppositely charged and separated by r is $\mathrm{d}C = \varepsilon_0 \mathrm{d}S/r$, where $\varepsilon_0 = 8.85 \times 10^{-12}\,\mathrm{C}^2\,\mathrm{N}^{-1}\,\mathrm{m}^{-2}$ is the vacuum permittivity.

On the other hand, the van der Waals energy, as well as Pauli's energy, due to the atomic interactions can be computed by using the well-known Lennard-Jones potential (Lennard-Jones, 1930). It presents an attractive term ($\propto r^{-6}$) describing the van der Waals forces and a repulsive one ($\propto r^{-12}$), due basically to Pauli's Principle. The effect of Pauli's Principle decays extremely fast and plays an important role only when the structures come into contact. As a consequence, it is dropped in the following discussion. To compute the total van der Waals energies, instead of the usual discrete approach, we can employ a continuum model (Girifalco et al., 2000;

Desquenes et al., 2002, 2004). In the continuum model, the total van der Waals energies are computed by the integral of the two terms in the Lennard-Jones potential, i.e.

$$E_{\mathrm{vdW}} = \int_{V_1}\int_{V_2} \frac{n_1 n_2 C_6}{r^6}\,\mathrm{d}V_1\,\mathrm{d}V_2, \tag{2}$$

where V_1 and V_2 represent the two volume domains of integration, $n_1$and n_2 are the corresponding atom densities and r is the distance between any point on V_1 and any point on V_2. C_6 is a material constant. For carbon–carbon interactions $C_6 = 15.2\ \mathrm{eV\mathring{A}}^6 = 2.43 \times 10^{-78}\,\mathrm{N\,m}^7$.

The component of the force along the r-direction can be derived from the corresponding energy terms as

$$F = -\frac{\mathrm{d}E}{\mathrm{d}r}. \tag{3}$$

3.2. Electrostatic and van der Waals energies per unit length

Following the approach discussed in the previous section, the electrostatic and van der Waals energies per unit length are (Desquenes et al., 2002)

$$\frac{\mathrm{d}E_{\mathrm{elec}}}{\mathrm{d}z} = \frac{\pi\varepsilon_0 V^2}{\cosh^{-1}(1 + r/R)}, \tag{4}$$

$$\frac{\mathrm{d}E_{\mathrm{vdW}}}{\mathrm{d}z} = \sum_{R=R_{\mathrm{int}}}^{R_{\mathrm{ext}}} \sum_{r=r_{\mathrm{int}}}^{r_{\mathrm{int}}+(N_G-1)d} \frac{\pi^2 C_6 n^2 d^2 R(r+R)(3R^2 + 2(r+R)^2)}{2((r+R)^2 - R^2)^{7/2}}, \tag{5}$$

where z is the axial co-ordinate of the cantilever nanotube ($z = 0$ at the clamp), R_{int} and $R \equiv R_{\mathrm{ext}}$ are the inner and outer radius of the (eventually multi-walled) nanotube, N_{G} is the graphene layer number of the substrate and d is the interlayer distance (for graphite $d = 0.335\,\mathrm{nm}$); in addition, $r \equiv r_{\mathrm{int}}$ is the gap between the nanotube (external wall) and the surface layer of the substrate, where n is the atomic density (e.g., for graphite $n = 1.14 \times 10^{29}\,\mathrm{m}^{-3}$).

The forces per unit length acting on the nanotube can be obtained by differentiating Eqs. (4) and (5) with respect to r as

$$q_{\mathrm{elec}} = -\frac{\mathrm{d}(\mathrm{d}E_{\mathrm{elec}}/\mathrm{d}z)}{\mathrm{d}r} \quad \text{and} \quad q_{\mathrm{vdW}} = -\frac{\mathrm{d}(\mathrm{d}E_{\mathrm{vdW}}/\mathrm{d}z)}{\mathrm{d}r},$$

as suggested by Eq. (3). The force q_{elec} is a consequence of the distributed charges in the nanotube. On the other hand, the charges will tend to have a concentration at the end of the nanotube, so that an additional force will act at the tip of the nanotube (Bulashevich and Rotkin, 2002; Ke and Espinosa, 2004). We will discuss this effect as well as the quantum correction with respect to the classical analysis in a latter section.

3.3. Total electrostatic and elastic energies stored in the nanotube

Let us consider, initially, the principal contribution to the pull-in voltage of the nanotube, i.e. the electrostatic forces. We start by assuming a uniform charge distribution. In addition, we reasonably assume that the nanotube's (external) radius R is much smaller than the distance r between nanotube and ground plane, i.e., $R/r \ll 1$. By this assumption Eq. (4) becomes

$$\frac{\mathrm{d}E_{\mathrm{elec}}}{\mathrm{d}z} \approx \frac{\pi\varepsilon_0 V^2}{\ln(2r/R)}. \tag{6}$$

Noting that $r = H - w$ (and $R/H \ll 1$) the electrostatic energy per unit length becomes

$$\frac{\mathrm{d}E_{\mathrm{elec}}}{\mathrm{d}z} = \frac{\pi\varepsilon_0 V^2}{\ln(2H/R)}\left(1 + \frac{1}{\ln(2H/R)}\sum_{i=1}^{\infty}\frac{1}{i}\left(\frac{w}{H}\right)^i\right). \tag{7}$$

We describe the deflection of the cantilever nanotube by using the following quadratic function,

$$w(z) \approx (1 + \varepsilon(z/L))\frac{z^2}{L^2}c, \tag{8}$$

where L is the length of the nanotube and c is an unknown constant that represents the displacement of the tip. The coefficient $\varepsilon(z/L)$ represents a correction to the assumed quadratic form, which is crucial only in the evaluation of the curvature of the beam. It means that we consider a quadratic form sufficient for describing displacements and rotations but not sufficient for describing the nonconstant curvature of the nanotube. Accordingly, it will be $1 \gg \varepsilon, \varepsilon' \ll \varepsilon''$, where the symbol $'$ represents differentiation with respect to the dimensionless variable z/L.

As a consequence, the elastic energy stored in the nanotube due to bending becomes

$$E_{\mathrm{elast}} = \frac{EI}{2}\int_0^L \left(\frac{\mathrm{d}^2 w}{\mathrm{d}z^2}\right)^2 \mathrm{d}z = \frac{2\xi EI}{L^3}c^2, \tag{9}$$

where the coefficient ξ arises from the integration of ε''. We estimate this coefficient, equating the maximum values of the elastic strain energy

$$E_{\mathrm{elast}} = \frac{EI}{2}\int_0^L \left(\frac{\mathrm{d}^2 w}{\mathrm{d}z^2}\right)^2 \mathrm{d}z$$

and that of the kinetic energy

$$K(t) = \frac{1}{2}\int_L \left(\frac{\mathrm{d}w}{\mathrm{d}t}\right)^2 \mu\,\mathrm{d}z$$

during its free vibration, i.e., $w(z,t) \approx (1 + \varepsilon(z/L))(z^2/L^2)c\sin\omega_0 t$. In these equations, μ is the nanotube mass per unit length and ω_0 is the well-known

fundamental frequency of the cantilever nanotube. The equality results in $\xi \approx \frac{1}{2}$. Accordingly, we will assume this value in the remainder of the analysis.

On the other hand, the total electrostatic energy stored in the nanotube, according to Eqs. (7) and (8), can be expanded in series as

$$E_{\text{elec}} = \int_0^L \frac{\mathrm{d}E_{\text{elec}}}{\mathrm{d}z}\,\mathrm{d}z = \frac{\pi\varepsilon_0 V^2 L}{\ln(2H/R)}\left(1 + \frac{1}{\ln(2H/R)}\sum_{i=1}^{\infty}\frac{1}{i(2i+1)}\left(\frac{c}{H}\right)^i\right). \tag{10}$$

3.4. Free energy, equilibrium and structural instability

The free energy (or total potential energy) of the system is

$$W(c) = E_{\text{elast}}(c) - E_{\text{elec}}(c). \tag{11}$$

The equilibrium condition is reached when the free energy reaches a minimum value, i.e., when $\mathrm{d}W(c)/\mathrm{d}c = 0$. On the other hand, a structural instability occurs at the so-called pull-in voltage, when $\mathrm{d}^2W(c)/\mathrm{d}c^2 = 0$.

3.4.1. Equilibrium

The equilibrium condition gives

$$V(c) = \frac{H}{L^2}\ln\left(\frac{2H}{R}\right)\sqrt{\frac{2EI}{\pi\varepsilon_0}}S_1\left(\frac{c}{H}\right), \tag{12a}$$

$$S_1\left(\frac{c}{H}\right) = \left\{\sum_{i=0}^{\infty}\frac{1}{(2i+3)}\left(\frac{c}{H}\right)^{i-1}\right\}^{-1/2}. \tag{12b}$$

The characteristic curve of Eq. (12), normalized with respect to the pull-in voltage, is given in Fig. 5. The descending branch could be experimentally captured only by a displacement-control device. On the other hand, if the NEMS is voltage-controlled, instead of the descending branch it will follow a horizontal line (at $V = V_{\text{PI}}$) until reaching the contact at $c/H = 1$. The difference between the two paths is related to the kinetic energy released by the structure after pull-in when the device is actuated under voltage-control.

3.4.2. Instability

According to Fig. 5, the instability, corresponding to the maximum of the curve, arises for

$$\left(\frac{c}{H}\right)_{\text{PI}} \approx \frac{2}{3}. \tag{13}$$

Note that since Eq. (13) is obtained by a second-order derivative, it could be considered only an estimate. However, the result is quite reasonable. The mean value (with respect to z) of the deflection is close to $(\langle w\rangle/H)_{\text{PI}} \approx \frac{1}{3}$, which is the same as the condition found in MEMS. On the other hand, in view of the fact that the

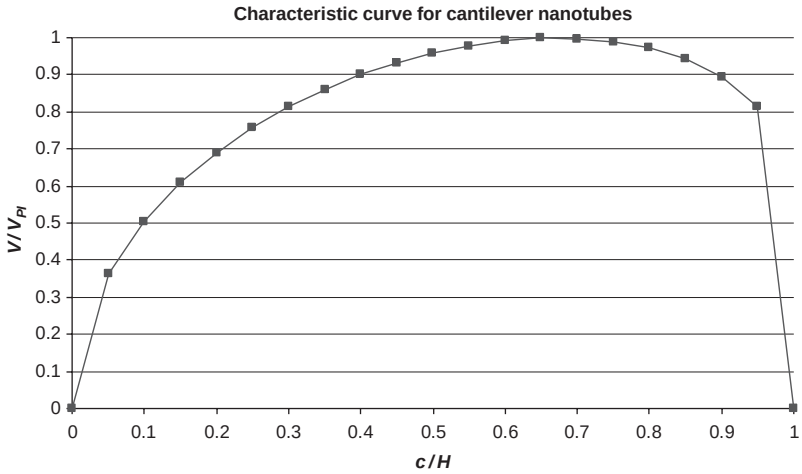

Fig. 5. Theoretical characteristic curve for cantilever nanotube.

characteristic curve is very flat near the maximum, the pull-in voltage may only be slightly affected by this ratio.

Substituting Eq. (13) into Eqs. (12a) and (12b) (the summation converges rapidly to $s_1(\frac{2}{3}) \approx 1.05$ gives the expression for the pull-in voltage of the nanotube as

$$V_{\mathrm{PI}} = k\frac{H}{L^2}\ln\left(\frac{2H}{R}\right)\sqrt{\frac{EI}{\varepsilon_0}}, \tag{14}$$

where theoretically $k \approx 0.85$.

As a consequence, the characteristic curve reported in Fig. 5 follows the expression

$$\frac{V(c)}{V_{\mathrm{PI}}} = 0.95 S_1\left(\frac{c}{H}\right). \tag{15}$$

Assuming that all the lengths are proportional to a characteristic length l, Eq. (14) shows that the pull-in voltage scales as $V_{\mathrm{PI}} \propto l$.

3.5. Correction due to the van der Waals forces

In this section we examine the effect of van der Waals forces as a correction to the pull-in voltage derived in the previous section. We also assess under what conditions such a correction becomes relevant.

According to our previous hypothesis, $R/r \ll 1$, Eq. (5) can be rewritten as

$$\frac{\mathrm{d}E_{\mathrm{vdW}}}{\mathrm{d}z} = \pi^2 C_6 n^2 d^2 N_W \langle R\rangle \sum_{r=r_{\mathrm{int}}}^{r_{\mathrm{int}}+(N_G-1)d} r^{-4}, \tag{16}$$

where N_W is the number of walls of the nanotube and $\langle R\rangle$ is the mean value of their radii.

Considering the first term in the series expansion of Eq. (16), we obtain

$$\frac{\mathrm{d}E_{\mathrm{vdW}}}{\mathrm{d}z} = \pi^2 C_6 n^2 d^2 N_W \langle R\rangle \sum_{i=0}^{N_G-1} (H+id)^{-4}\left(1-\frac{w}{H+id}\right)^{-4}$$
$$\approx \pi^2 C_6 n^2 d^2 N_W \langle R\rangle \sum_{i=0}^{N_G-1} (H+id)^{-4}\left(1+4\frac{w}{H+id}\right), \tag{17}$$

in which we have neglected terms $O(w/(H+id))^2$.

By employing Eqs. (8) and (17), the total van der Waals energy accumulated in the tube is

$$E_{\mathrm{vdW}} = \int_0^L \frac{\mathrm{d}E_{\mathrm{vdW}}}{\mathrm{d}z}\,\mathrm{d}z = \pi^2 C_6 n^2 d^2 L N_W \langle R\rangle \sum_{i=0}^{N_G-1} (H+id)^{-4}\left(1+\frac{4}{3}\frac{c}{H+id}\right). \tag{18}$$

The variation of the van der Waals energy during a variation of the deflection of the nanotube yields

$$\frac{\mathrm{d}E_{\mathrm{vdW}}}{\mathrm{d}c} = \tfrac{4}{3}\pi^2 C_6 n^2 d^2 L N_W \langle R\rangle S_2, \tag{19a}$$

$$S_2 = \sum_{i=0}^{N_G-1} (H+id)^{-5}. \tag{19b}$$

To derive simple formulas, we evaluate the summation S_2 in Eq. (19b) assuming a small number i of layers, i.e., $H+id \approx H$

$$S_2 \approx \frac{N_{\mathrm{G}}}{H^5}, \tag{20a}$$

or a large number of layers, by substituting the summation with an integral,

$$S_2 \approx 4\int_0^{N_G} (H+id)^{-5}\,\mathrm{d}i = \frac{1}{4d}\left(\frac{1}{H^4}-\frac{1}{(H+N_G d)^4}\right), \tag{20b}$$

that for a very large number of layers (semi-infinite ground plane) it becomes

$$S_2 \approx \frac{1}{4dH^4}. \tag{20c}$$

Comparing Eqs. (20c) and (20a) defines precisely what we mean by a *large number of layers*, i.e., $N_{\mathrm{G}}^* \approx H/4d$. Accordingly, the equilibrium condition gives

$$V^{\mathrm{vdw}}(c) = V(c) - \Delta^{\mathrm{vdw}} V(c), \tag{21a}$$

$$\Delta^{\mathrm{vdW}} V(c) = nd\,\ln\left(\frac{2H}{R}\right)\sqrt{\frac{4\pi C_6 H N_W \langle R\rangle S_2}{3\varepsilon_0}}\,S_1\left(\frac{c}{H}\right)\sqrt{\frac{c}{H}}, \tag{21b}$$

where $V(c)$ is again given by Eq. (12). V^{vdW} is the voltage including van der Waals forces and ΔV^{vdW} is the correction arising from these forces. At first glance, the

correction to the characteristic curve due to the van der Waals forces seems to be negligible due to the very small value of the constant C_6. However, from Eq. (21) we can infer its effect on the characteristic curve of a device and the corresponding pull-in voltage.

Noting that the pull-in voltage is slightly dependent on the ratio c/H, the correction can be simply estimated substituting $(c/H)_{\mathrm{PI}} \approx \frac{2}{3}$ in Eq. (21b), which yields

$$\Delta^{\mathrm{vdW}} V_{\mathrm{PI}} \approx 2nd \ln\left(\frac{2H}{R}\right)\sqrt{\frac{C_6 H N_W \langle R\rangle S_2}{\varepsilon_0}}. \tag{22}$$

This correction scales as $\Delta^{\mathrm{vdW}} V_{\mathrm{PI}} \propto l^{-1}$ (assuming a semi-infinite ground plane) and becomes dominant with respect to the electrostatic contribution $V_{\mathrm{PI}} \propto l$ as the size l approaches zero.

3.6. Correction due to nonlinear kinematics

In this section we examine the effect of nonlinear kinematics as a correction to the pull-in voltage formula derived in Section 3.4. Under large displacements we assume for the deflection of the nanotube the following form:

$$w(s) \approx (1 + \varepsilon(s/L))\frac{s^2}{L^2}c, \tag{23}$$

where s is the natural co-ordinate along the longitudinal axis of the nanotube and $1 \gg \varepsilon, \varepsilon' \ll \varepsilon''$. Only for small displacements $s \approx z$. Under this assumption, the total electrostatic and van der Waals energies

$$E_{\mathrm{elec}} = \int_0^L \frac{\mathrm{d}E_{\mathrm{elec}}}{\mathrm{d}s}\,\mathrm{d}s, \tag{24}$$

$$E_{\mathrm{vdW}} = \int_0^L \frac{\mathrm{d}E_{\mathrm{vdW}}}{\mathrm{d}s}\,\mathrm{d}s \tag{25}$$

are the same as those reported in Eqs. (9) and (10). The advantage of the assumption of Eq. (23) (with respect for example to $w(z) \approx (z^2/(L-\Delta)^2 c)$, with Δ being the horizontal tip displacement) is that the effect of the finite kinematics appears only in the elastic energy E_{elast}.

Noting that $\mathrm{d}s^2 = \mathrm{d}z^2 + \mathrm{d}w^2$, and making use of Eq. (23) and considering the first corrective term we obtain

$$\left(1 - \frac{2c^2}{L^4}s^2 - \frac{2c^4}{L^8}s^4\right)\mathrm{d}s \cong \mathrm{d}z. \tag{26}$$

Integrating Eq. (26) we obtain

$$\int_0^L \left(1 - \frac{2c^2}{L^4}s^2 - \frac{2c^4}{L^8}s^4\right)\mathrm{d}s \cong \int_0^{L-\Delta} \mathrm{d}z, \tag{27}$$

which yields the horizontal displacement Δ of the tip:

$$\Delta \cong \frac{2}{3}\frac{c^2}{L}. \tag{28}$$

This result is important for a better description of the tip vector position (Δ, $w(s=L)$) of NEMS designed for large displacement applications.

The elastic energy stored in the nanotube is

$$E_{\text{elast}} = \frac{EI}{2}\int_0^L \left(\frac{\mathrm{d}\vartheta}{\mathrm{d}s}\right)^2 \mathrm{d}s, \tag{29}$$

where ϑ defines the slope of the elastic line of the nanotube. Noting that, from Eq. (26),

$$\left(1-\frac{2c^2}{L^4}s^2-\frac{2c^4}{L^8}s^4\right) \cong \frac{\mathrm{d}z}{\mathrm{d}s} = \cos\,\vartheta \cong 1-\frac{\vartheta^2}{2}, \tag{30}$$

we obtain

$$\vartheta \cong \frac{2c}{L^2}s\sqrt{1+\frac{c^2}{L^4}s^2} \cong \frac{2c}{L^2}s\left(1+\frac{c^2}{2L^4}s^2\right). \tag{31}$$

Hence, Eq. (29) yields

$$E_{\text{elast}} = \frac{2\xi EIc^2}{L^3}\left(1+\frac{c^2}{L^2}\right), \tag{32}$$

where ξ arises from the integration of ε''. The first term is the classical one related to small displacements; therefore, the second term represents the correction due to large displacements.

Differentiating Eq. (32) with respect to c and comparing the result with Eq. (9), one finds

$$EI \to \left(1+\frac{2c^2}{L^2}\right)EI. \tag{33}$$

As a result, the characteristic curve including finite kinematics is given by Eq. (12a) with the substitution identified by Eq. (33). Hence,

$$V^{\text{FK}}(c) \approx \sqrt{1+\frac{2c^2}{L^2}}\frac{H}{L^2}\ln\left(\frac{2H}{R}\right)\sqrt{\frac{2EI}{\pi\varepsilon_0}}S_1\left(\frac{c}{H}\right). \tag{34}$$

Eq. (34) being also a function of c/L, cannot be plotted solely in terms of c/H, as was done for the characteristic curve reported in Fig. 5. However, we can discuss two limit cases. One case corresponds to $H/L \to 0$. The correction is negligible and we obtain the result discussed in Section 3.4. The other limit case, $H/L \to 1$, corresponds to contact under large deflections. The two limit cases (Eq. (34) with $c/L \to 0$ or $c/L \to c/H$) are compared in Fig. 6. We can observe that a larger deflection is experienced by the system before the onset of instability. Accordingly,

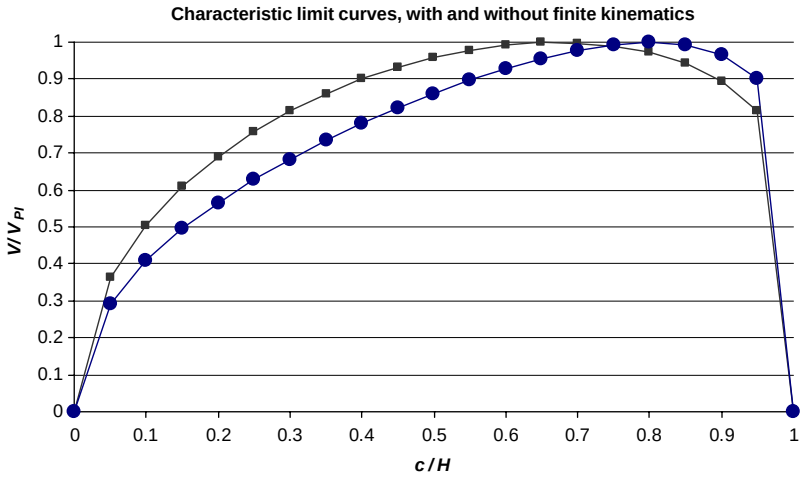

Fig. 6. Effect of the finite kinematics on the theoretical characteristic curve of the nanotube cantilever. Squares correspond to the case H/L approaching zero and circles correspond to the case $H/L = 1$.

the pull-in is predicted by

$$V_{\mathrm{PI}}^{\mathrm{FK}} = \sqrt{1 + \beta \frac{H^2}{L^2}} V_{\mathrm{PI}}, \tag{35}$$

where V_{PI} is again given by Eq. (14) and neglecting the small variation of $c/H, \beta \approx \frac{8}{9}$.

It is interesting to note that the correction due to the van der Waals forces, in which the term EI does not appear, does not affect the correction due to the finite kinematics.

3.7. Free-end charge concentration and quantum effects

It is well known that at the ends of a linear conductor charges tend to concentrate. The same effect happens in a cantilevered nanotube. Even when its influence could be considerable, it is not usually taken into account. This section aims to evaluate this effect.

We start by assuming a concentration in charge Q_0 at the end of the nanotube of length$L \gg H, R$ (Ke and Espinosa, 2004):

$$Q_0 = \frac{2K\pi\varepsilon_0 V}{\cosh^{-1}(1 + r/R)}, \tag{36}$$

where $K \approx 0.85(R(H+R)^2)^{1/3}$, which has a length unit ($\sim L$).

According to Eqs. (4) and (1),

$$E_{\substack{\mathrm{elec} \\ \mathrm{con}}} \approx K \frac{\pi\varepsilon_0 V^2}{\cosh^{-1}(1 + r/R)}, \tag{37}$$

which represents the additional electrostatic energy concentrated at the end of the nanotube. Here $r = H - c$ is the distance between nanotube tip and electrode. Considering $r \gg R$ and differentiating Eq. (37) with respect to c gives

$$\frac{\mathrm{d}E_{\underset{\text{con}}{\text{elec}}}}{\mathrm{d}c} \approx K \frac{\pi\varepsilon_0 V^2}{H(1-c/H)\ln^2((2H/R)(1-c/H))}. \tag{38}$$

The equilibrium will be reached for a minimum of the free energy, which in this case is given by $W(c) = E_{\text{elast}}(c) - E_{\text{elec}}(c) - E_{\text{vdW}}(c) - E_{\underset{\text{con}}{\text{elec}}}(c)$. According to Eq. (38) the correction on the characteristic curve given by Eq. (12a) can be easily taken into account by the following substitution:

$$\ln\left(\frac{2H}{R}\right) \to \ln\left(\frac{2H}{R}\right)\left(1 + K\frac{\ln^2(2H/R)}{L(1-c/H)\ln^2((2H/R)(1-c/H))}\right)^{-1/2}. \tag{39}$$

Considering $(c/H)_{\text{PI}} \approx \frac{2}{3}$, the pull-in voltage of Eq. (14) decreases, becoming

$$V_{\text{PI}}^{\text{con}} = \left(1 + 3K\frac{\ln^2(2H/R)}{L\ln^2(2H/3R)}\right)^{-1/2} V_{\text{PI}}. \tag{40}$$

It is interesting to note that the correction due to the concentration of charges does not affect the other corrections. As a consequence, for large displacements instead of V_{PI}, in Eq. (40) we have to employ $V_{\text{PI}}^{\text{FK}}$. The correction due to the van der Waals forces remains described by Eq. (22) in which we have to make the substitution described by Eq. (38).

In addition, Bulashevich and Rotkin (2002) suggest a quantum correction for the capacitance per unit length, i.e., for the electrostatic energy, of the form of

$$\frac{\mathrm{d}E_{\text{elec}}^{Q}}{\mathrm{d}z} \approx \frac{\mathrm{d}E_{\text{elec}}}{\mathrm{d}z}\left(1 - \frac{1}{2\ln(2r/R)e^2 v_{\text{M}}}\right), \tag{41}$$

where v_{M} is the constant density of the states near the electroneutral level measured from the Fermi level. We can evaluate accordingly the quantum correction, yielding an increase of the pull-in voltage as

$$V_{\text{PI}}^{\text{Q}} \approx V_{\text{PI}}\left(1 - \frac{1}{2\ln(4H/3R)e^2 v_{\text{M}}}\right)^{-1/2}. \tag{42}$$

The correction (42) still neglects the transverse polarization of the nanotube, reasonable for the usual cases, for which

$$\frac{R^2}{4H^2\ln(2H/R)} \ll 1.$$

4. Comparison between analytical predictions and experiments

In this section, a comparison between analytical predictions and experimental data, for both small deformation and finite kinematics regimes, is presented.

4.1. Small deformation regime

The nanotweezers experimental data reported by Akita et al. (2001) is plotted in Fig. 7. The nanotweezer is equivalent to a nanotube cantilever with a length of 2.5 μm freestanding above an electrode with a gap of 390 nm. The experimentally measured pull-in voltage was 2.33 V. In the same figure, a comparison between the analytically predicted nanotube cantilever deflection and the experimentally measured data is shown. The analytical model includes the van der Waals force and charge concentration at the free end of the nanotube cantilever. Model parameters include Young's modulus, $E = 1$ TPa, external radius $R = R_{ext} = 5.8$ nm, and $R_{int} = 0$. The pull-in voltage from our analytical model is 2.34 V. It is clear that the analytical prediction and experimental data for the deflection of the nanotube cantilever, as a function of applied voltage, are in good agreement. The estimated radius of the nanotube by Akita et al. and Desquesnes et al. was 6.65 nm and 5.45 nm, respectively. The value identified by our detailed analysis falls in between and is consistent with possible metrology errors.

4.2. Finite kinematics regime

The experimentally measured nanotube cantilever deflections, in the finite kinematics regime, are plotted in Fig. 8 (see Section 2.2). The figure also shows a

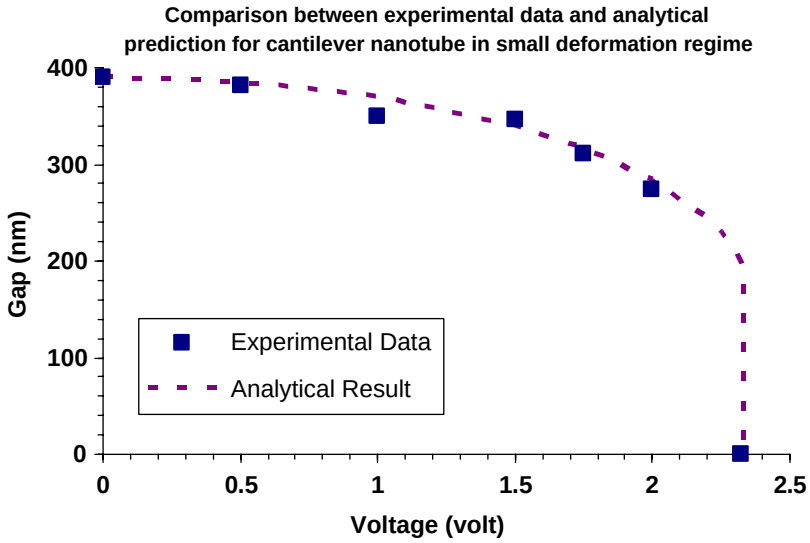

Fig. 7. Comparison between experimental data and theoretical prediction in the small deformation regime.

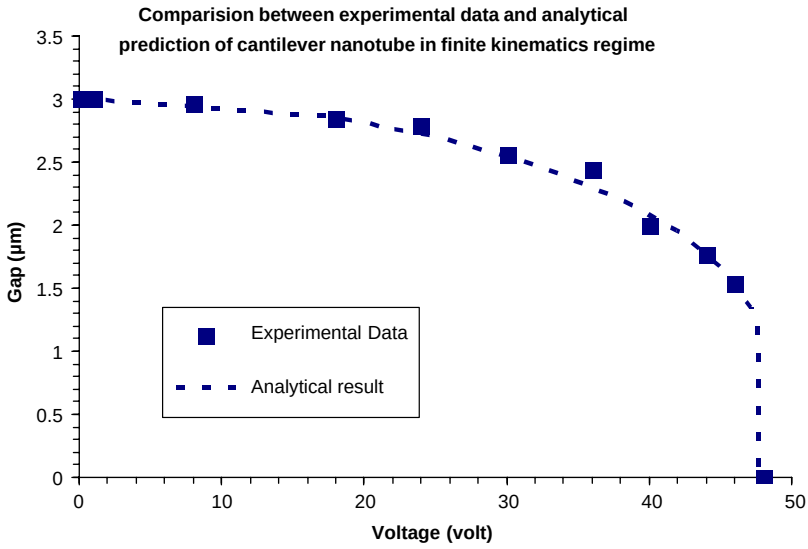

Fig. 8. Comparison between experimental data and theoretical prediction in the finite kinematics regime.

comparison between analytical prediction and experimental data. The analytical model includes finite kinematics, the van der Waals force and charge concentration at the free end of the nanotube cantilever. For these predictions, the following parameters were employed: length of the nanotube, $L = 6.8\,\mu\text{m}$, initial gap between nanotube and electrode, $H = 3\,\mu\text{m}$, $R = R_{\text{ext}} = 23.5\,\text{nm}$, $R_{\text{int}} = 0$, $E = 1\,\text{TPa}$. The pull-in voltage from the analytical analysis is 47.8 V, while the pull-in voltage experimentally measured is 48 V. It is clear that the experimental and theoretical predictions are in good agreement. It should be noted that the value of R_{ext} was estimated from high-magnification SEM images.

5. Closure

We have investigated carbon nanotube-based NEMS devices and, in particular, the electrostatic actuation of cantilever nanotubes by means of both experiments and modeling in the small deformation and finite kinematics regimes. The experimental measurements of nanotube cantilever deflection in the finite kinematics regime are the first of their kind. Likewise, for the first time an analytical model is derived, which is able to describe the local and global deformation of the nano structure as a function of applied voltage. The model takes into account the cylindrical shape of the deflected nanotube, in the evaluation of its electrical capacitance, the influence of the van der Waals forces, large kinematics, as well as the concentrated charge in the free end of the nanotube cantilever. Comparisons between analytical predictions and experimental results in both regimes show excellent agreement within the resolution

of SEM metrology. Of all the effects contributing to the deformation and pull-in of the device, the concentration of charge at the end of the cantilever was identified as the most dominant, with an error of 13.4% when its effect is omitted. The finite kinematics effect is less pronounced, with an error of 7.0% when neglected. These errors were computed for the geometry and material examined in our experiments.

The methodologies here reported are completely general and as such are expected to be useful in the characterization of electromechanical properties of nanotubes and nanowires, as well as in the optimal design of nanotube-based NEMS devices.

Acknowledgements

The authors acknowledge the support from the FAA through Award no. DTFA03-01-C-00031 and the NSF through Award no. CMS-0120866. We would like to express our appreciation to Drs. J. Newcomb and J. Larsen-Base for supporting this work. Work was also supported in part by the Nanoscale Science and Engineering Initiative of the National Science Foundation under NSF Award no. EEC-0118025. The pull-in test was carried out in the Center for Microanalysis of Materials, University of Illinois, which is partially supported by the US Department of Energy under Grant DEFG02-91-ER4543. The authors would like to acknowledge N. Moldovan for providing insightful suggestions.

References

Akita, S., et al., 2001. Nanotweezers consisting of carbon nanotubes operating in atomic force microscope. Appl. Phys. Lett. 79, 1691–1693.

Bulashevich, K.A., Rotkin, S.V., 2002. Nanotube devices: a microscopic model. JETP Lett. 75, 205–209.

Chopra, N.G., Zettl, A., 1998. Measurement of the elasticity of a multi-wall boron nitride nanotube. Sol. State. Comm. 105, 297–300.

Desquenes, M., Rotkin, S.V., Aluru, N.R., 2002. Calculation of pull-in voltages for carbon nanotube-based nanoelectromechanical switches. Nanotechnology 13, 120–131.

Desquenes, M., Tang, Z., Aluru, N.R., 2004. Static and dynamic analysis of carbon nanotube-based switches. J. Eng. Mater. Technol. 126, 230–237.

Fennimore, A.M., Yuzvinsky, T.D., Han, W.-Q., Fuhrer, M.S., Cumings, A., 2003. Rotational actuators based on carbon nanotubes. Nature 424, 408–410.

Girifalco, L.A., Hodak, M., Lee, R.S., 2000. Carbon nanotubes, buckyballs, ropes, and a universal graphitic potential. Phys. Rev. B 62, 104–110.

Iijima, S., 1991. Helical microtubules of graphitic carbon. Nature 354, 56–58.

Johnson, H.T., Liu, B., Huang, Y.Y., 2004. Electron transport in deformed carbon nanotubes. J. Eng. Mater. Technol. 126, 222–229.

Ke, C.-H., Espinosa, H.D., 2004. Numerical analysis of nanotube based NEMS devices. Part I: electrostatic charge distribution on multiwalled nanotubes, J. Appl. Mech., accepted for publication.

Kim, P., Lieber, C.M., 1999. Nanotube nanotweezers. Science 286, 2148–2150.

Lennard-Jones, J.E., 1930. Perturbation problems in quantum mechanics. Proc. R. Soc. A 129, 598–615.

Liu, B., Jiang, H., Johnson, H.T., Huang, Y.Y., 2004. The influence of mechanical deformation on the electrical properties of single wall carbon nanotubes. J. Mech. Phys. Solids 52, 1–26.

Qian, D., Wagner, G.J., Liu, W.K., Yu, M.-F., Ruoff, R.S., 2002. Mechanics of carbon nanotubes. Appl. Mech. Rev. 55, 495–532.

Rueckes, T., Kim, K., Joselevich, E., Tseng, G.Y., Cheung, C.-L., Lieber, C.M., 2000. Carbon nanotube-based nonvolatile random access memory for molecular computing. Science 289, 94–97.

Tombler, T., Zhou, C., Alexeyev, L., Kong, J., Dai, H., Liu, W., Jayanthi, C., Tang, M., Wu, S.Y., 2000. Reversible nanotube electro-mechanical characteristics under local probe manipulation. Nature 405, 769–772.

Treacy, M.M., Ebbesen, T.W., Gibson, J.M., 1996. Exceptionally high Young's modulus observed for individual carbon nanotubes. Nature 381, 678–680.

Yakobson, B.I., Campbell, M.P., Brabec, C.J., Bernholc, J., 1997. High strain rate fracture and C-chain unraveling in carbon nanotubes. Comp. Mat. Sci. 8, 341–348.

Yu, M.-F., Lourie, O., Dyer, M.J., Moloni, K., Kelly, T.F., Ruoff, R.S., 2000. Strength and Breaking Mechanics of Multiwalled Carbon Nanotubes Under Tensile Load. Science 287, 637–640.